Fabrication and characterization of Zn–ZnO core–shell microspheres from nanorods

O. Lupan [a,b,*], L. Chow [a], G. Chai [c], H. Heinrich [a,d]

[a] Department of Physics, University of Central Florida, P.O. Box 162385 Orlando, FL 32816-2385, USA
[b] Department of Microelectronics and Semiconductor Devices, Technical University of Moldova, Stefan Cel Mare Boulevard 168, Chisinau MD-2004, Republic of Moldova
[c] Apollo Technologies, Inc. 205 Waymont Court, S111, Lake Mary, FL 32746, USA
[d] Advanced Materials Processing and Analysis Center, and Department of Mechanical, Materials, and Aerospace Engineering, University of Central Florida, Orlando, FL 32816, USA

ARTICLE INFO

ABSTRACT

We present a new method to synthesize ZnO nanorods on zinc spheres to form a core–shell structure. Selective self-assembly growth of a shell with ZnO nanorods on a metallic Zn microsphere core has been accomplished via hydrothermal synthesis. The crystal structure, morphologies and chemical composition were characterized by X-ray diffraction, transmission electron microscopy, scanning electron microscopy and energy dispersive X-ray spectroscopy. The interfacial chemistry involved in the growth of ZnO nanorods on the Zn core and a possible growth mechanism are discussed. The specific structure of the highly oriented one-dimensional nanorods may find applications in nanoelectronics, nanophotonics and nanomedicine.

1. Introduction

The controlled fabrication of functional nanoarchitectured materials is an important objective of fundamental and applied research. In nanotechnology, it is important to synthesize specifically shaped nanostructures, which could serve as building blocks in the assembly process. There are different synthesis techniques that are used for the surface coating of an object, such as sol-gel coating, self-assembly and sonochemical processing.

Among all the nanomaterials, ZnO attracted a lot of attention with its various architectures [1,2], as an excellent candidate for self-assembly. ZnO is also promising for device applications due to its unique material properties such as wide and direct band gap and a large free exciton binding energy [3], high optical gain $(300 \, cm^{-1})$ [4,5] and high mechanical and thermal stabilities [6,7]. ZnO nanorods with their high carrier mobility serve as direct conduction pathways for excitons and they can represent different types of nanoscale building blocks that have been used to assemble functional devices [1–4,8–10]. Especially important for applications of these ZnO one-dimensional (1-D) nanorods are methods to assemble them into highly integrated and hierarchically organized nanostructures for device integration without using sophisticated equipment [4–8].

Core/shell type ZnO nano/microspheres have been studied due to their potential applications in nanocomposite materials. For example, Sulieman et al. [11] have reported a vapor transport synthesis of hollow-opened ZnO/Zn or Zn/ZnO microspheres on Si sub-strate using high purity Zn and ZnO powder as sources. Duan et al. [12], employed an integrated autoclave and pyrolysis process to synthesize partially opened ZnO hollow microspheres. In both cases, high temperatures (600 °C or higher) were used to react the Zn powder with oxygen and the ZnO shells are consisted of multicrystalline domains or particulates.

Here, we report for the first time a simple hydrothermal synthesis of self-assembled ZnO nanorods into three-dimensional (3-D) spherical shells on a Zn microsphere. The ZnO nanorods are self-organized such that their c-axes are all perpendicular to the surface of the Zn microsphere and the length of the ZnO nanorods is equivalent to the thickness of the ZnO shell. We also propose a possible growth mechanism and discuss factors that influence the formation mechanism of the ZnO nanorods shell on Zn core.

2. Experimental

2.1. Synthesis

An appropriate quantity of zinc sulfate [$Zn(SO_4) \cdot 7H_2O$] and ammonium hydroxide [$NH_4(OH)$] (Fisher Scientific, 99.9%) were mixed until they were completely dissolved. The molar ratio of Zn^{2+}/NH_3 was in the range 1:2 to 1:20. The pH of the system was 10.5. The aqueous solution was loaded into a reactor [13] and a piece of cleaned silicon wafer or cleaned glass substrate [14] was placed in the aqueous solution and 0.3–1.0 g of pure zinc powder (2–10 μm in diameter) was added. Then the reactor was transferred and positioned on a hot plate [13]. The system was heated to a preset temperature (95 °C) and held for 15 min.

Initially, zinc sulfate was dissolved in deionized water. Then by adding ammonia solution, it dissociated in water [15].

* Corresponding author. Address: Department of Physics, University of Central Florida, P.O. Box 162385 Orlando, FL 32816-2385, USA. Fax: +1 407 823 5112.
E-mail address: lupan@physics.ucf.edu (O. Lupan).

The initial solution contains milky colored precipitates of zinc hydroxide at a low concentration of ammonia,

$$Zn^{2+} + 2OH^- \Longleftrightarrow Zn(OH)_2, \ K_{SP} = 3 \times 10^{-17} \tag{1}$$
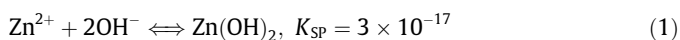
where K_{SP} is the solubility product constant. After adding ammonium hydroxide, zinc hydroxide starts to form Zn complex. The solution becomes clear when the molar ratio of Zn^{2+}/NH_3 is 1:4. By increasing temperature, zinc ions are complexed by OH^- and form $[Zn(OH)_4]^{2-}$ and $[Zn(NH_3)_4]^{2+}$ in ammonia solution. A pH > 10 condition and an aqueous environment are crucial keys in ensuring the formation of the growth unit of $(Zn(OH)_4)^{2-}$ and a controlled release of the units from solution:

$$Zn(OH)_2 + 2(OH)^- \rightarrow (Zn(OH)_4)^{2-} \tag{2}$$
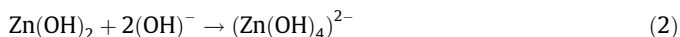
The concentration of OH^- in the solution is a key factor for the control of the growth rate of different crystal faces. It can lead to the formation of an anisotropic shaped object such as nanorod assembled shell observed here.

Increasing the temperature of the complex solution leads to the formation of zinc oxide after reaction took place:

$$Zn(OH)_2 \xrightarrow{\text{hydrothermal process}} ZnO + H_2O \tag{3}$$
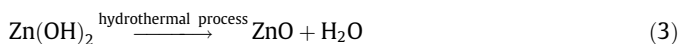
During the hydrothermal process [16], zinc complexes also dissociate and dehydrate to form ZnO directly. Thus, ZnO is formed by decomposing:

$$[Zn(OH)_4]^{2-} \xrightarrow{\text{hydrothermal process}} ZnO + H_2O + 2OH^- \tag{4}$$
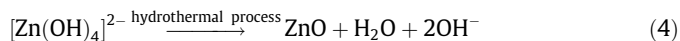
and for ammonia complex with zinc ions:

$$[Zn(NH_3)_4]^{2+} + 2OH^- \xrightarrow{\text{hydrothermal process}} ZnO + 4NH_3 + H_2O \tag{5}$$
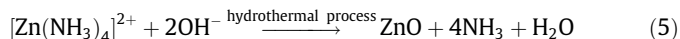
where NH_3 is one of the byproducts that will prevent amalgamation of the nucleus in supersaturated solution during the reaction process and lead to a dispersed morphology [16].

Finally, the whole system is allowed to cool down to room temperature. The substrates are dipped and rinsed in deionized water and then the samples are dried in air at 150 °C for 5 min.

2.2. Characterization

X-Ray diffraction (XRD) measurements were carried out on a Rigaku 'D/B max' instrument operating at a voltage of 40 kV and a current of 30 mA with CuK_α radiation (λ = 1.54178 Å). All samples were measured in a continuous scan mode at 10–90° (2θ) with a scanning rate of 0.01°/s. The morphology images of the samples were obtained using a scanning electron microscope (SEM, JEOL), the composition was measured by energy dispersion X-ray spectroscopy (EDX). Transmission electron microscopy (TEM) and selected area electron diffraction (SAED) measurements were performed on a FEI Tecnai F30 TEM transmission electron microscope operated at an accelerating voltage of 300 kV. A TEM cross-sectional sample was prepared using a focused ion beam (FIB) system FEI 200TEM. The micro-manipulator inside the FIB/SEM chamber is used to assist pick-up the TEM cross-sectional sample and mount it on a Cu grid.

3. Results

Fig. 1 shows the X-ray diffraction pattern of the as-prepared samples. Peak positions and relative intensities for synthesized Zn/ZnO core–shell microspheres were compared to values from Joint Committee on Powder Diffraction Standards (JCPDS) card for ZnO (JCPDS 036-1451) [17] and for Zn (JCPDS PDF #00-004-0831) [17].
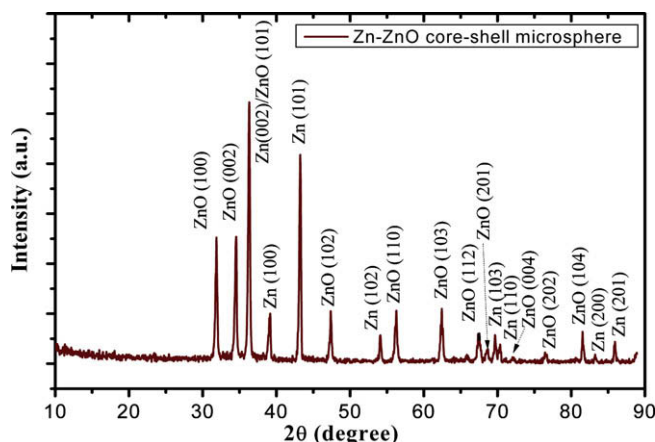

Fig. 1. The XRD patterns of the as-synthesized Zn/ZnO core–shell microspheres.

The XRD pattern of Zn/ZnO core–shell microspheres depicted in Fig. 1 confirms that the shells of the samples are composed of Wurtzite ZnO nanorods (JCPDS 036-1451) [17]. The sharpness of the diffraction peaks indicates high crystallinity of the as-grown samples. All peaks are accounted for either from ZnO or pure Zn metal. No characteristic peak of other chemical compounds was observed.

The composition of the Zn/ZnO core–shell microspheres was investigated by an EDX system attached to the TEM. Fig. 2a shows the results from a cross section of an individual core–shell structure covered with Pt film and mounted on a TEM Cu grid. Results imply that the samples contain only Zn and O in the shell without other impurities within the detection limits of EDX (Fig. 2b and c). Fig. 2d indicates that the core contains only pure Zn. The copper (Cu) peak in Fig. 2c and d comes from the copper grid on which the Zn/ZnO core–shell microspheres were mounted.

The morphologies of the as-synthesized samples were characterized by scanning electron microscopy (SEM). Fig. 3a and b are typical SEM images of the Zn powder and of the Zn/ZnO core/shell microsphere, respectively. As shown in Fig. 3a the original morphology of the Zn powder is spherical with diameters ranging from 2 to 10 μm.

In Fig. 3b and c, the as-grown Zn/ZnO core–shell structure is spherical with diameters varying between 3 μm and 12 μm and possesses three-dimensional radial symmetry. These microspheres are loosely bound to the substrate and the growth process is independent of the substrate. A closer examination of the structures shown in Fig. 3b indicates that all ZnO nanorods have hexagonal cross-section, which confirms that 1-D growth is directed along the c-axis according to XRD results. Careful observation on samples shows that the surfaces of these spheres are built by 1-D nanorods with radii ranging from 100 nm to 200 nm (Fig. 3b and c). By increasing the zinc ions concentration in solution, the 1-D nanorods grow denser on the shell (Fig. 3c). The shape of the microspheres is very uniform. The spheres cut with FIB are fully filled with the nanorods as shown in Fig. 3d. The cut spheres show the dense nature of the products. The thickness of these ZnO nanorod shells is estimated from the cross-section (Fig. 3d) to be about 1–2 μm.

Additional structural characterization of the as-synthesized ZnO spheres was carried out by TEM using selected area electron diffraction. The atomic structure of the ZnO nanorod/Zn core heterojunction was investigated with the use of a high-resolution TEM (HRTEM).

Fig. 4a shows the TEM image from Zn/ZnO spheres and Fig. 4b and c the corresponding SAED images. The SAED pattern of the Zn core is shown in Fig. 4b. The electron diffraction pattern
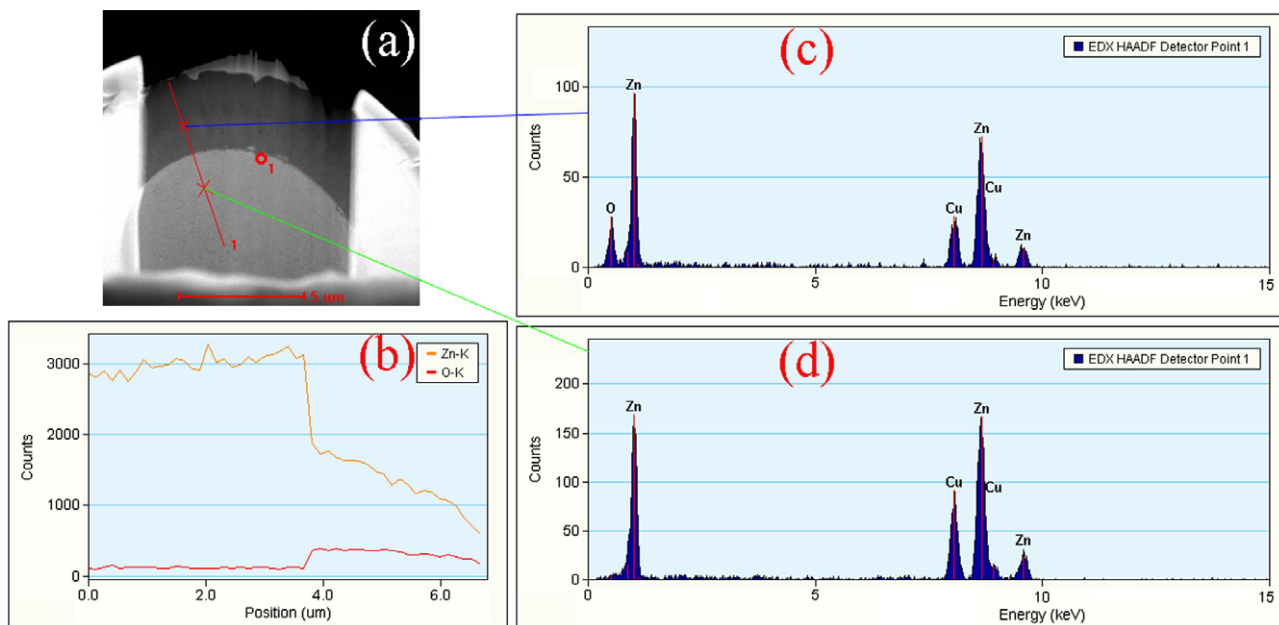
Fig. 2. (a) Cross-sectional view of Zn/ZnO core–shell microsphere cut in focused ion beam system and mounted on a TEM Cu grid and showing regions for EDX analysis. EDX patterns: (b) linescan along the scanned path (red line in a) of Zn core/ZnO 1-D nanorods shell covered with a Pt film in the FIB system and (c) of the ZnO nanorod shell of the microspheres. (d) Of the Zn core. Cu peaks in EDX spectra (c,d) are from the copper grid. (For interpretation of the references to color in this figure legend, the reader is referred to the web version of this article.)
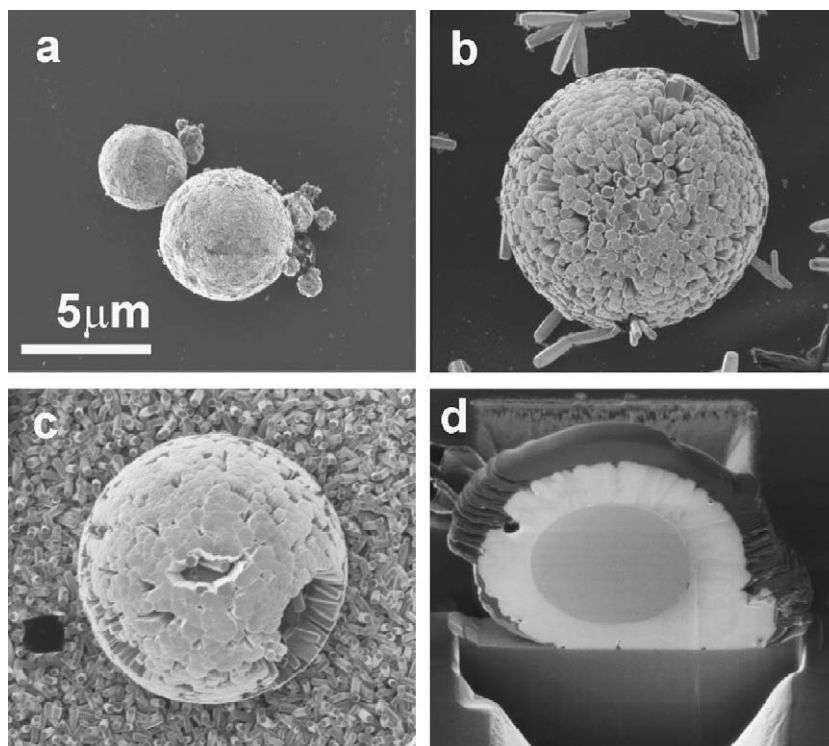

Fig. 3. (a) A typical SEM image of the Zn core spheres. (b–c) SEM images corresponding to the ZnO nanorods shell/Zn core grown at different concentration ratio Zn^{2+}/OH^{-}, respectively. (d) SEM image from junction ZnO/Zn cross-sectional view. All scale bars are the same for (a–d).

(Fig. 4c) of the ZnO spheres indicates that the ZnO shell is formed by single crystal nanorods with growth direction along the c-axis.

Fig. 4a shows the typical structure of the ZnO nanorod/Zn core nanojunction. The SAED images of the square-marked sections (b) and (c) are presented in Fig. 4b (Zn core) and c (ZnO nanorod), respectively. Fig. 4c shows the crystalline ZnO nanorod growth along the [0 0 0 1] direction, indicating that the (1 1 1) fringes perpendicular to the wire axis are. The SAED pattern in Fig. 4c, which was obtained from the nanorod, can be indexed according to the hexagonal ZnO structure.
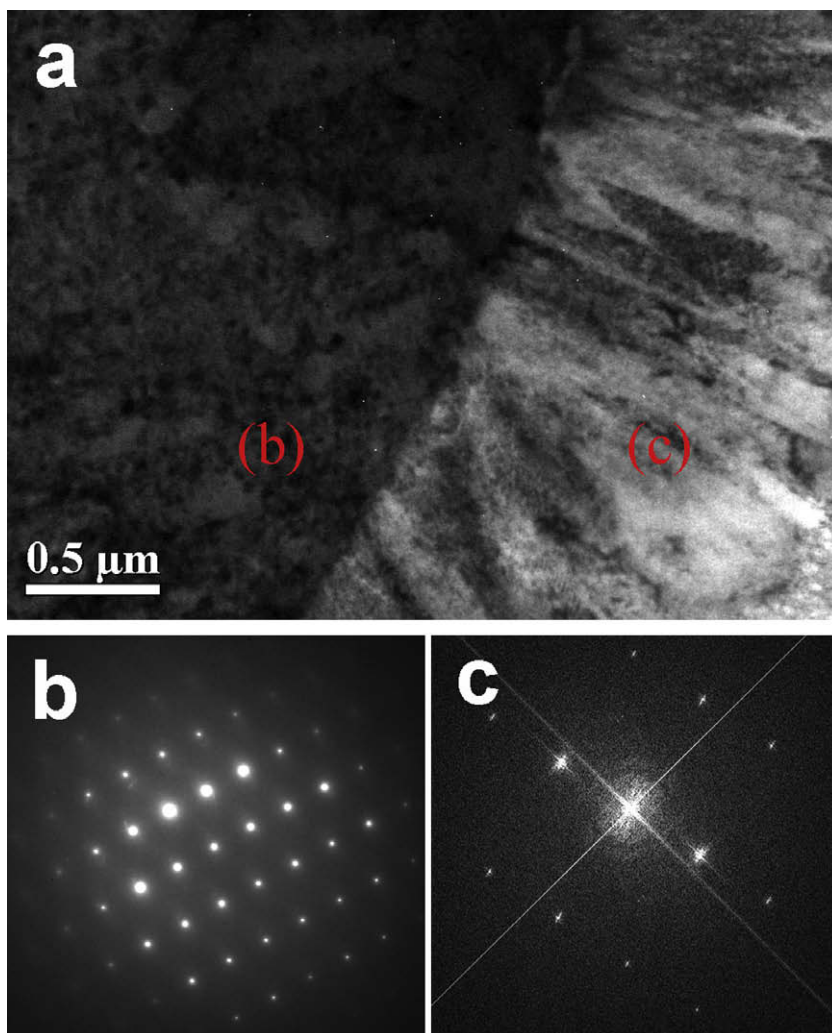
Fig. 4. (a) A typical TEM image of the Zn core/ZnO nanorods shell heterojunction. (b) Selected area electron diffraction patterns (SAED) obtained from Zn core and (c) SAED of ZnO nanorods shell, respectively.

4. Discussion

According to our experimental results of the morphological and structural characterizations of Zn/ZnO microspheres, the ZnO nanorods growth on the Zn sphere can be understood on the basis of the growth mechanism proposed below.

Although the dual roles of ammonia Eqs. (1) and (5)) in ZnO synthesis can be explained, the formation mechanism of ZnO 1-D nanorods shell on Zn metal core could be more complicated. The proposed mechanism of growth of Zn/ZnO core–shell spheres via hydrothermal self-assembly is proposed in Scheme 1.

At the beginning of the growth, the Zn sphere acts as a nucleation site and the – OH^- ions start to attach to the surface (like 'dandelion') of the Zn microsphere. Zn^{2+} and OH^- ions are further supplied by hydration process of zinc sulfate and ammonia, respectively. $Zn(OH)_2$ is formed (Eq. (1)) and subsequently transformed to ZnO (Eq. (3)) as the initial nucleation site for ZnO nanorods (Scheme 1). When the solution is supersaturated, nucleation begins. Further ZnO nanorods are continuously formed on this nucleation layer from Zn^{2+} and OH^- (Scheme 1). The concentration of OH^- in solution is a key factor in controlling the growth rate of different crystal faces. This morphology is mainly attributed to the
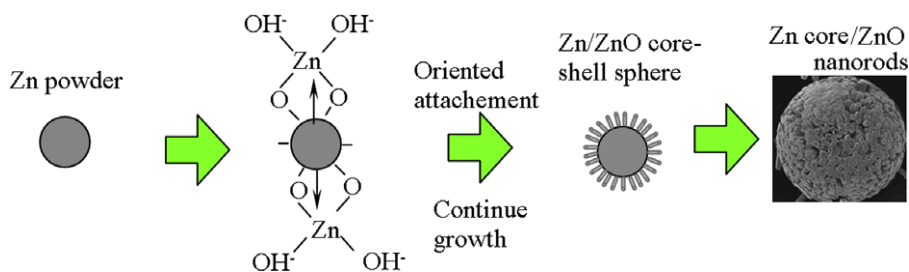
Scheme 1. Schematic illustration of the growth mechanism of Zn/ZnO solid core–shell microsphere.

basicity afforded by (NH_3) and $[Zn(NH_3)_4]^{2+}$, which cause the growth along the c-axis at a higher rate than along any other axis to form regular hexagonal shapes [16]. Since the (0001) faces have higher-symmetry (C_{6v}) than other faces growing along the $+c$-axis ($[0001]$ direction), this is the typical growth plane. ZnO nanorods grow preferentially along the $[0001]$ direction also because the new (0001) planes are formed easily [18] and all nanorods have the same length, which makes a perfectly shape sphere. The (0001) plane is the highest energy plane in crystal, thus attaching to the (0001) plane is energetically favorable. The molecules at the surface are energetically less stable than the ones already well ordered and packed in the interior. The nucleation determines the surface-to-volume ratio of the ZnO nanorod. Then, incorporation of growth units into the crystal lattice of the nanorods by dehydration reaction takes place. It is concluded that the growth mechanism is determined by thermodynamic factors and by the concentration of OH^- – as the kinetic factor in aqueous solution growth.

Due to the high density of nanorods on Zn sphere, steric hindrance effects [19,20] can have a direct influence on the radial alignment of ZnO nanorods shell. In ZnO structures, each Zn atom is bound with four O atoms and forming a tetrahedral configuration (Scheme 1). Zn leans to the (0001) plane and O to the $(000\bar{1})$. Due to the fact that a ZnO crystal is a polar crystal, O^{2-} is in the hexagonal closest packing and in this case each Zn^{2+} lies within a tetrahedral group of four oxygen ions (Scheme 1). Thus zinc and oxygen atoms have been arranged along the c-axis. The formation rate of new (0001) planes is faster than the growth rate within the (0001) planes, leading to pointed tips of the nanorods.

5. Conclusion

In summary, self-assembled shells of ZnO nanorods have been successfully grown on a Zn powder core using a hydrothermal process. The microspheres exhibit spherical shapes and their shell consisted of self-assembled ZnO 1-D nanorods. A smooth surface of the Zn core is covered with ZnO 1-D nanorods which are forming a shell. EDX and XRD analysis show that Zn/ZnO microspheres are of high purity with Wurtzite structure, and the ZnO 1-D nanorods are single crystalline with the c-axis as the growth direction.

The ZnO nanorods are perpendicularly grown on the surface of the Zn core with a unique orientation relationship with respect to the substrate and exhibit a very narrow size distribution ($\sim$20 nm for ZnO nanorods) with edges parallel to the $[100]$ and $[010]$ directions of ZnO. The formation of coherent 3-D nanorods is governed by the minimization of the free energy involving the inter-play between surface energy and elastic strain energy contribution. The growth of 3-D nanorods in ZnO can be affected by the growth temperature and ratio Zn^+/OH^-.

To summarize, a technique for localized growth and alignment of ZnO nanorods on Zn powder core substrates to yield a self-assembled system has been demonstrated. This process with its improved control yields a simple and reproducible method, which could be used in fabrication of nanodevices.

References

[1] P.X. Gao, Z.L. Wang, J. Appl. Phys. 97 (2005) 044304.
[2] O. Lupan, L. Chow, G. Chai, A. Schulte, S. Park, O. Lopatiuk-Tirpak, L. Chernyak, H. Heinrich, Superlattices Microstruct. 43 (2008) 292.
[3] D.G. Thomas, J. Phys. Chem. Solids 15 (1960) 86.
[4] Y. Chen, D.M. Bagnall, H. Koh, K. Park, K. Hiraga, Z. Zhu, T. Yao, J. Appl. Phys. 84 (1998) 3912.
[5] A. Ohtomo et al., Mater. Sci. Eng. B 56 (1998) 263.
[6] R.C. Wang, C.P. Liu, J.L. Huang, S.-J. Chen, Y.-K. Tseng, Appl. Phys. Lett. 87 (2005) 013110.
[7] J. Wang, L. Gao, Solid State Commun. 132 (2004) 269.
[8] W. Park, S.W. Jung, G. Yi, S.H. Oh, C.G. Park, M. Kim, Jpn. J. Appl. Phys. 41 (2002) L1206.
[9] O. Lupan, G. Chai, L. Chow, Microelectron. J. 38 (2007) 1211.
[10] L. Chow, O. Lupan, G. Chai, V. Sontea, Self-Assembly Arrayed One-Dimensional ZnO Nanorods by Hydrothermal Technique; 2008 NSTI Nanotechnology Conference and Trade Show, June 1–5, 2008, Boston, Massachusetts, USA, <http://www.nsti.org/Nanotech2008/showabstract.html?absno=1691>.
[11] K.M. Sulieman, X.T. Huang, J.P. Liu, M. Tang, Nanotechnology 17 (2006) 4950.
[12] J.X. Duan, X.T. Huang, E.K. Wang, H.H. Ai, Nanotechnology 17 (2006) 1786.
[13] O. Lupan, L. Chow, G. Chai, B. Rodan, A. Naitabdi, A. Schulte, H. Heinrich, Mater. Sci. Eng., B 145 (2007) 57.
[14] O. Lupan, S. Shishiyanu, L. Chow, T. Shishiyanu, Thin Solid Films 516 (2008) 3338.
[15] I. Oladeji, L. Chow, Thin Solid Films 339 (1999) 148.
[16] J. Zhang, L.D. Sun, J.L. Yin, H.L. Su, C.S. Liao, C.H. Yan, Chem. Mater. 14 (4) (2002) 172.
[17] Joint Committee on Powder Diffraction Standards, Powder Diffraction File No 036-1451 and #00-004-0831.
[18] W.J. Li, E.W. Shi, W.Z. Zhong, Z.W. Yin, J. Cryst. Growth 203 (1999) 186.
[19] Z.F. Ren, Z.P. Huang, J.W. Xu, J.H. Wang, P. Bush, M.P. Siegal, P.N. Provencio, Science 282 (1998) 1105.
[20] C.J. Lee et al., Chem. Phys. Lett. 312 (1999) 461.